Joint Synchronization and Demodulation by Forward Filtering

Murthy V. R. S. Devarakonda
Email: murthyds@ieee.org

Hans-Andrea Loeliger
ETH Zurich
Email: loeliger@isi.ee.ethz.ch

Abstract—In a typical receiver, symbol synchronization must be established before symbol demodulation. This paper discusses synchronization for an isolated symbol from a filter-bank type multicarrier system. It is shown that accurate symbol timing for a single multicarrier symbol can be obtained using forward-only processing. The proposed receiver computes continuous-time symbol likelihoods along with a timing metric and its time derivative. The timing metric shows a sharp concentration that is used to produce a trigger to sample the matched filter outputs. The paper proposes baseband processing using message passing algorithms derived from factor graphs. Suitable system parameters for which near-optimum synchronization is obtained are identified using computer simulations.

I. Introduction

In a typical receiver, symbol synchronization must be established before symbol demodulation, which, in turn, must precede decoding. Synchronization is particularly challenging when isolated packets are transmitted at times unknown to the receiver. The established approaches in this case can be classified into two groups. In the first approach, the data is preceded by a preamble that enables the receiver to synchronize before demodulation. In the second approach, the whole block is first sampled asynchronously and digitally stored, and then processed to figure out the symbol boundaries. Neither of these approaches is entirely satisfactory: the first approach wastes transmission energy for the preamble, whereas the second approach requires much digital processing.

In this paper, we propose a new approach to this problem. For a suitably defined multicarrier symbol format, we show that symbol synchronization (for an isolated symbol that arrives at an unknown time) can be obtained as a by-product of matched filtering. The receiver in the proposed system has the general structure shown in Fig. 1: a time-invariant "filter" produces, first, a continuous-time likelihood vector $L(t)$ and simultaneously, a timing signal $L_{\mathcal{T}0}(t)$ and its derivative, from which a trigger signal is generated to sample the likelihood signal $L(t)$ at an optimal moment. The "filter" may be either a continuous-time analog circuit or a discrete-time digital processing unit with a free-running clock; the notation that we will use assumes the latter, but the proposed system is perfectly suitable for implementation in the former mode. Unlike OFDM, the proposed approach does not use a cyclic prefix, and the symbol does not need to arrive within a fixed time window. For other approaches to the synchronization of multicarrier symbols see, e.g., [1] [2].
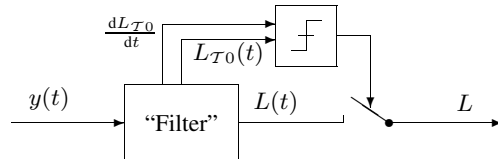

Fig. 1. Demodulation (i.e., computation of symbol likelihoods L) and synchronization as a byproduct of matched filtering.

The paper is structured as follows. The system setup is introduced in Sec. II. Sec. III provides an overview of likelihood filters [3] based on linear Gaussian state-space models, message passing on Forney-style factor graphs, and puts together various ideas – in particular, localized models for pulses using *glue factors* – to define a framework for receiver processing. Synchronization and detection with forward processing are elaborated in Sec. IV and performance results are provided for different combinations of system parameters in Sec. V. The paper is concluded in Sec. VI. The description of the likelihood computations in Sec. III will assume some familiarity with Forney-style factor graphs as in [4].

II. System Setup

Fig. 2 shows the system set up. The transmitter modulates an encoded block, $(b_1, \ldots, b_M) \in \{+1, -1\}^M$, of M bits, on to binary antipodal pulses. The transmit signal is,

$$\phi[j] = \sum_{m=1}^{M} \alpha_m \operatorname{Re}\{\phi_{CB}[j] \exp(i\Omega_m j)\}, -J \le j \le 0, \quad (1)$$

where $\alpha_m, m = 1, \ldots, M$ are real and $|\alpha_m|$ are known amplitudes, $b_m\alpha_m > 0$, $\phi_{CB}[j]$ is a complex baseband pulse, and the elementary pulses are located in adjacent frequency bands with $\Omega_m = (m-1)\Omega_0$. We assume orthogonality among the elementary pulses. We consider baseband processing, assuming perfect carrier recovery. The receiver sees a noisy version of the delayed signal: $y_j = \phi[j - \nu_0] + z_j$, where z_j are i.i.d, zero mean Gaussian random variables with variance σ^2 and ν_0 is the delay unknown to the receiver. The received signal is passed through a bank of filters whose outputs are used to compute two statistics. At the outputs denoted as Ⓐ, time-varying log-likelihood ratios for the symbols are produced. From the outputs denoted as Ⓑ, the overall signal-to-noise log-likelihood ratio is computed which is used to detect the packet, and to provide a trigger to sample the symbol likelihoods. It is well known that the accuracy of pulse position
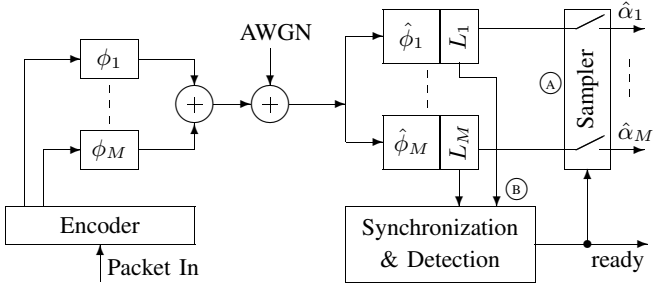
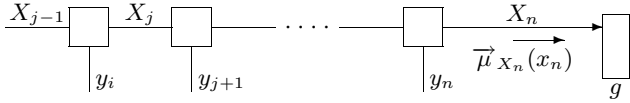Fig. 2. Block diagram of multicarrier transceiver.

Fig. 3. Factor graph of a constrained state space model.

estimation improves with the number of dimensions [5]. When M is sufficiently large, the likelihood for the received signal exhibits a sharp concentration around the ideal sampling time ν_0. This phenomenon is fundamental to the scheme and is used to sample the bits on the fly as the signal arrives and provide soft outputs $(\hat{\alpha}_1, \ldots, \hat{\alpha}_M)$ to a decoder.

III. LIKELIHOOD COMPUTATION WITH FACTOR GRAPHS

We are interested in computing the likelihood for a state-space model using the Forney style factor graph shown in Fig. 3 with observations $y = (y_1, \ldots, y_n)$, and hidden state sequence $X = (X_1, \ldots, X_n)$. While the following discussion applies to general state-space models, we restrict ourselves to autonomous (i.e., without input) linear models and Gaussian noise with scalar observations: $X_k = AX_{k-1}$, $S_k = CX_k$, $Y_k = S_k + Z_k$, $Z_k \sim \mathcal{N}(0, \sigma^2)$, where A, B, and C are matrices of suitable dimensions (our notation closely follows [4]). The graph imposes a constraint on the state vector at time n using a *glue factor* [3] labeled g. For example, for a pure sinusoid model, by choosing $g(x_n) \propto \delta(\|x_n\| - 1)$, the factor graph effectively models a subclass of sinusoids on the unit circle. By placing the glue factor always at the current time instance, n, we obtain a *time-varying* hypothesis, denoted as $\mathcal{H}(n, g)$. The graph represents the joint density $p(y, X|\mathcal{H}(n, g))$. Using sum-product message passing, the likelihood of the observations under the hypothesis $\mathcal{H}(n, g)$ can be obtained as,

$$p(y|\mathcal{H}(n, g)) = \int_x p(y, x_1, x_2, \ldots, x_n|\mathcal{H}(n))g(x_n, \theta)\,\mathrm{d}x,$$

$$= p(y|\mathcal{H}(n)) \int_{x_n} \overrightarrow{f}_{X_n}(x_n)g(x_n, \theta)\,\mathrm{d}x_n, \quad (2)$$

where $p(y|\mathcal{H}(n))$ is the likelihood of the unconstrained model (g is absent), $\overrightarrow{f}_{X_n}(x_n)$ is the *normalized* forward message, $\overrightarrow{\mu}_{X_n}(x_n)$, and $g(x_n, \theta)$ is parametrized by θ. From (2) we note that the forward message is a sufficient statistic for θ.

When matrix A is non-singular, the choice of the glue factor $g(x_n, \theta) = \delta(x_n - \theta)$ completely determines the state
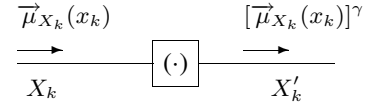

Fig. 4. State forgetting.

trajectory. In this case, we obtain the likelihood for the *known signal* hypothesis. Message passing with this choice leads to many useful properties that enable us to derive algorithms with forward processing as highlighted below.

a) The *known signal* likelihood can be written as $p(y|\mathcal{H}(n, g)) = p(y|\mathcal{H}(n))\overrightarrow{f}_{X_n}(x_n = \theta)$. By choosing different parameters θ_1 and θ_2, likelihoods for different hypotheses, such as in a binary signaling scheme, can be obtained simultaneously using the same model.

b) The *noise only* hypothesis can be obtained with $\theta = 0$, as this implies an all zero solution for the state sequence.

c) In some problems, the previous two results lead to like-lihood ratio computations using only forward messages because the unconstrained likelihood $p(y|\mathcal{H}(n))$ cancels out. For example, the likelihood ratio between signal and noise hypotheses is $\overrightarrow{f}_{X_n}(x_n = \theta)/\overrightarrow{f}_{X_n}(x_n = 0)$, that between two known signal hypotheses is $\overrightarrow{f}_{X_n}(x_n = \theta_1)/\overrightarrow{f}_{X_n}(x_n = \theta_2)$, and so on.

d) ML parameter estimation can now be restated using (2) as $\theta_{\mathrm{ML}} = \mathrm{argmax}_\theta \overrightarrow{f}_{X_n}(\theta)$.

e) For a linear Gaussian model, the known signal-to-noise log-likelihood ratio is related to the inner product as (see [6] for details),

$$L_{\mathcal{A}0}[n] = \frac{1}{2\sigma^2}\left[2\left\langle y[\cdot], \tilde{\phi}[\cdot - \kappa]\right\rangle - \|\tilde{\phi}\|^2\right], \quad (3)$$

where $\tilde{\phi}$ is the underlying known signal modeled by some glue factor parameter θ. It is important to note that, for glue factor at time n, the delay, κ, can be controlled by a suitable choice of θ. As we are going to show, this can be used to delay the computations to the end of a signal (a time-limited pulse in our case) until all energy has been received. We obtain this using forward computations and do not require the signal to be causal.

The description so far assumed a finite observation window. To obtain algorithms in a truly forward processing style, we introduce some approximations.

A. Likelihood Filters from Localized Models

Gaussian message passing requires computation of the mean vector, $\overrightarrow{m}_{X_n}$, and the covariance matrix, $\overrightarrow{V}_{X_n}$. By modifying the message computations as shown in Fig. 4 for every edge X_k, we introduce a "forgetting" with $0 < \gamma < 1$. The update rule for the covariance matrix in this case typically has a steady state solution, $V_\infty = \lim_{n\to\infty} \overrightarrow{V}_{X_n}$. By using V_∞, and by taking the lower limit of summation to $X_{-\infty}$ in (2), the message updates for $\overrightarrow{m}_{X_n}$ can be performed in the form of a stable filter. This has the effect of localizing the model to the immediate past with an exponential window, and is controlled by γ. From the likelihood filter, the two key parameters, $\overrightarrow{m}_{X_n}$ and V_∞ of the Gaussian message, $\overrightarrow{f}_{X_n}(x_n)$,

are readily available for extracting various likelihoods.

B. Modeling Pulses

We consider approximating a time-limited pulse as a sum of L sinusoids: $\phi[j] \simeq \sum_{\ell=1}^{L} \alpha_\ell \cos(\Omega_\ell j + \psi_\ell), -\frac{J}{2} \leq j \leq \frac{J}{2}$. Many pulses of practical interest, viz. a root-raised cosine Nyquist pulse or a Gaussian pulse, are well approximated with $L = 5$. This decomposition can be written using a separate state-space model for each sinusoid: at time k, we have $X_{\ell,k} = A_\ell X_{\ell,k-1}$, $S_k = \sum_{\ell=1}^{L} C_\ell X_{\ell,k}$. This leads to a loopy factor graph (due to the sum term). An approximation to message passing is to avoid the message iterations around the sum term (the details are omitted here). In other words, each model assumes the observations $y_k = C_\ell X_{\ell,k} + Z_k$ (instead of $y_k = S_k + Z_k$) by ignoring the contribution from the other models. This approximation does not lead to substantial performance loss.

When the pulse decomposition is combined with localized models, we obtain a bank of filters from which time-varying likelihoods can be computed. For a single pulse, LLR for a known signal-to-noise hypothesis can be written as,

$$L_{\mathcal{A}0}[n] = \sum_{\ell=1}^{L} \left[\overrightarrow{m}_{X_{\ell,n}}^T \overrightarrow{W}_\ell \theta_\ell - \frac{1}{2}\theta_\ell^T \overrightarrow{W}_\ell \theta_\ell \right], \qquad (4)$$

where $\overrightarrow{W}_\ell$ is inverse of the steady state covariance matrix for the ℓ-th model.

For forward processing, the delay mentioned with respect to equation (3) is controlled by choosing, e.g., $C_\ell = [1, 0]$, $\theta_\ell = \left[\alpha_\ell \cos(\frac{\Omega_\ell J}{2} + \psi_\ell), \alpha_\ell \sin(\frac{\Omega_\ell J}{2} + \psi_\ell) \right]^T$. The resulting LLR is depicted for two pulses in Fig. 5. The plots to the left show a transmitted RRC pulse in baseband (top) and the LLR in (4) delayed to the end of the pulse (bottom). The plots to the right correspond to another RRC pulse shifted in frequency. The optimum sampling time is at $\frac{J}{2}$, where the models match the transmitted signals in each case.

When the pulses are used in binary antipodal signaling as in (1), the LLR, $L_m[n]$, for each bit is,

$$L_m[n] = \sum_{\ell=1}^{L} 2\overrightarrow{m}_{X_{\ell,n}^m}^T \overrightarrow{W}_{m,\ell} \theta_{m,\ell}, \quad m = 1, \ldots, M, \quad (5)$$

where the indices $m = 1, \ldots, M$ and $\ell = 1, \ldots, L$ refer to the ℓ-th state-space model for the m-th transmit pulse, ϕ_m. Parameters $\theta_{m,\ell}$ correspond to the bit hypothesis $b_m = +1$. When the message passing approximation is combined with localized models, the uncoded BER for binary antipodal signaling (with perfect symbol timing) for a single RRC pulse is about 0.2dB worse compared to the theoretical limit. For the multicarrier system in (1), the uncoded BER suffers a further loss of about 0.3 to 0.5dB. This is due to the loss of orthogonality of the pulses arising out of the approximations.

IV. SYNCHRONIZATION AND DETECTION

The problem of receiving a single multicarrier symbol described in Section I is two fold: to detect the presence of the transmit signal, and to identify the unknown delay ν_0 to sample the matched filter outputs in Fig. 2 using forward
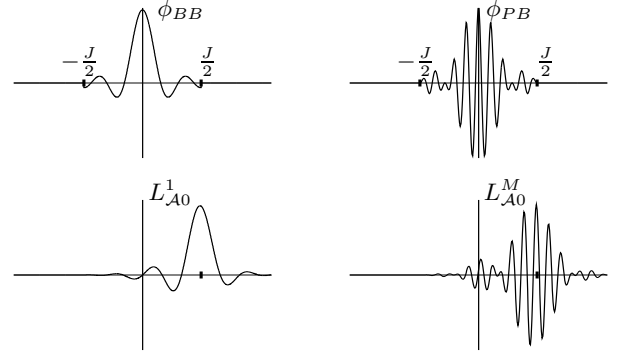

Fig. 5.   Signal versus noise LLRs for RRC pulses.

processing. The problem of finding the best sampling time when the data is unknown (non-data aided synchronization) is equivalent to identifying the pulse position when the pulse parameters are unknown. For convenience we assume that the transmit pulse ends at time 0 and a noisy version is received with an unknown delay ν_0. The maximum likelihood estimate of the pulse position, ν_{ML}, can be obtained from the log-likelihood ratio of the total transmit pulse versus noise hypothesis, $L_{\mathcal{T}0}[\nu]$, with $\nu_{\mathrm{ML}} = \mathrm{argmax}_\nu L_{\mathcal{T}0}[\nu]$, and

$$L_{\mathcal{T}0}[\nu] = \sum_{m=1}^{M} \max_{\rho_m} L_{m0}[\nu, \rho_m], \qquad (6)$$

where $\rho_m \triangleq (\theta_{m,1}, \ldots, \theta_{m,L})$ is the parameter vector for the hypothesis $b_m = +1$ and the maximization is over $\{+\rho_m, -\rho_m\}$. The LLRs $L_{m0}[\nu, \rho_m]$ for individual pulses are computed by adapting (4) to each model. Sampling the bit LLRs at ν_{ML} does not necessarily result in a well performing system unless the ML estimate is very good. In the following, we examine this from two angles. First, we examine how ν_{ML} depends on M and the total pulse energy, E_{T}. Second, we consider whether a reliable detection using a thresholding algorithm (for forward processing) is feasible. Throughout this section, we consider RRC pulses located in adjacent frequency bands as in (1).

A. Dependency of ν_{ML} on M and SNR

We examine how the ML timing estimation error, $\nu_\epsilon \triangleq \nu_{\mathrm{ML}} - \nu_0$, depends on M and the total SNR E_{T}/N_0. E_{T} refers to the energy of the transmitted pulse, ϕ; as M increases, the energy per bit, E_b, of the individual pulses is proportionally decreased to keep E_{T} normalized to unity to enable a fair comparison of the contribution due to M. Fig. 6 shows the average squared timing error (ASE) when the pulse parameters are fully known (i.e., the $\max_{\rho_m}$ in (6) is replaced with known values of ρ_m). The plots (dot-dashed lines) show an improvement in ASE when M is increased. Fig. 6 also shows (solid lines) the ASE for the unknown parameter case, which is our interest. The gain with M is not very pronounced at low SNRs. However, for a given choice of E_b (M), increasing M (E_b) leads to an increase of pulse energy E_{T}, helping to reduce the ASE within some required range. Secondly, the
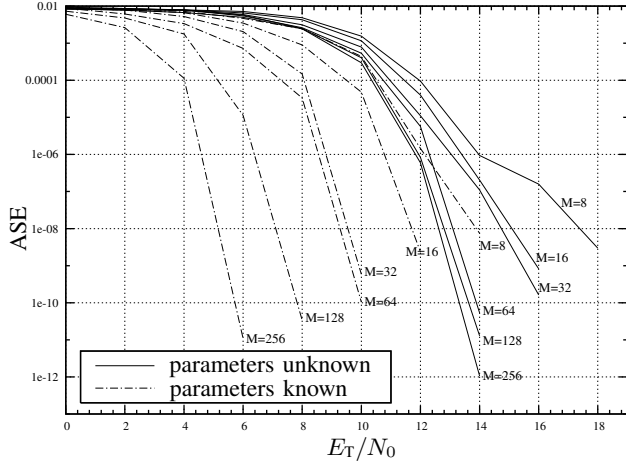
Fig. 6.   Timing ASE versus SNR.

Fig. 8.   Threshold choices for $L_{\mathcal{T}0}[\nu]$.

TABLE I
DESIGN TOLERANCES FOR ML DETECTION

M	$f_{max} = \frac{\Omega_{max}}{2\pi T_s}$	$\Delta\nu_{max}$ ($\theta_{max} < 2$ degree)	$\sigma^2_{\Delta\nu}$ max. allowed	$\left(\frac{E_b}{N_0}\right)_{min}$ dB
64	3190	1.74155e-06	1.89563e-13	7.6
128	6390	8.69414e-07	4.72425e-14	5.3
256	12790	4.34367e-07	1.17921e-14	2.7

time-varying LLR, $L_{\mathcal{T}0}[\nu]$ shows a sharp concentration around ν_0 for $M > 64$ as depicted in Fig. 7. These two properties can be used to achieve timing synchronization.

B. Threshold Detection and Synchronization

We would like to exploit the concentration depicted in Fig. 7 by sampling the bit-wise LLRs when $L_{\mathcal{T}0}[\nu]$ crosses a threshold L_{thr}. This is shown in Fig. 8. If the threshold is low, shown as L_{thr_1}, an early detection occurs, resulting in the packet being dropped eventually by the receiver. The threshold can be raised, say, to L_{thr_2} to detect very close to ν_{ML}, but this would increase the probability of missed detection. A feasible choice depends on the statistics of the LLR a little away from the peak, at $L_{\mathcal{T}0}[\nu_{ML} - \epsilon]$, and close to the peak, at $L_{\mathcal{T}0}[\nu_{ML}]$. We introduce the term "false detection" in this context:

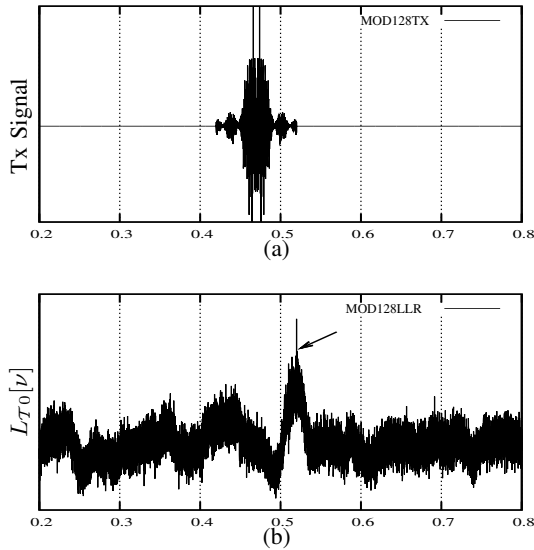**Definition. False Detection.** False detection is defined as detecting a noisy pulse at a time outside a specified limit,

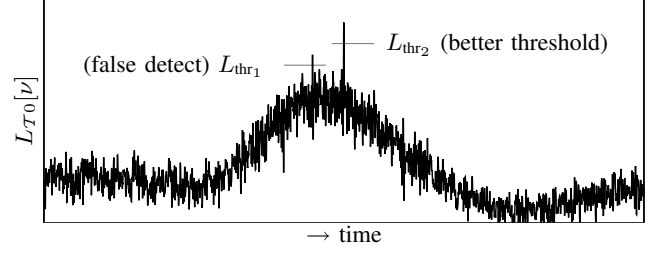Fig. 7.   Concentration of $L_{\mathcal{T}0}$ for large M.

$\Delta\nu_{max}$. Detection at time $\hat{\nu}$ is classified as a false detection if $|\hat{\nu} - \nu_0| > \Delta\nu_{max}$.

False detects dominate the system performance and the false alarm condition (detecting a signal when none is present) is less important in this system. Two types of events contribute to false detects. Event **E1** is caused by the ML timing estimation error, $|\nu_{ML} - \nu_0| > \Delta\nu_{max}$. This error can be reduced only by increasing either M or E_b or both. Event **E2** is the LLR in the region away from the peak crossing the threshold as shown in Fig. 8. Another error condition is missed detections arising from $L_{\mathcal{T}0}[\nu_{ML}]$ falling below the threshold. A suitable operating point meets a given set of criteria for the timing error, and probabilities for false and missed detection.

C. Choice of System Parameters

The system parameters M, E_b, and the receiver threshold L_{thr} can be obtained as outlined below. As timing error affects sampling of the pulses placed higher up on the spectrum, we allow up to a certain phase error, θ_{max}, in the state space model corresponding to the highest frequency, Ω_{max}:

$$|\nu_{ML} - \nu_0| \leq \Delta\nu_{max}, \text{ where } \Delta\nu_{max} = \theta_{max}/\Omega_{max}, \quad (7)$$

When M is large, the ML timing estimation error $\Delta\nu = \nu_{ML} - \nu_0$ is nearly Gaussian. As an example, by choosing, $\Delta\nu_{max} > 4\sigma_{\Delta\nu}$, the probability of false detection (due to the timing error event **E1**) is upper bounded as, $\Pr\{\Delta\nu > \Delta\nu_{max}\} < \Pr\{\Delta\nu > 4\sigma_{\Delta\nu}\} = 3.167 \times 10^{-5}$. $\Delta\nu_{max}$ depends on M via Ω_{max}. Table I shows design parameters for $\theta_{max} = 2$ degrees, and a minimum value of E_b/N_0 that meets the criterion (7).

When M is large, $L_{\mathcal{T}0}[\nu_{ML}]$ also tends to be nearly Gaussian. Given a probability of missed detection, p_{md}, we can choose L_{thr} such that

$$\Pr\{L_{\mathcal{T}0}[\nu_{ML}] < L_{thr}\} < p_{md}. \quad (8)$$

The above criterion is sufficient because, $L_{\mathcal{T}0}[\nu_{ML}] \geq L_{\mathcal{T}0}[\nu], \forall \nu$. A feasible operating point (M and E_b) is one which meets (7) and (8). This implies in general a further increase in E_T via either M, or E_b, or both compared to the operating points given in Table I.

V. RESULTS

We compare the performance of two detection algorithms with the algorithm using ML position estimates. In the first algorithm, a fixed offset is added to the detected threshold to adjust for a bias:

Threshold Detection "THR":

- Identify the time $\hat{\nu}$ at which the LLR crosses a threshold: $L_{\mathcal{T}0}[\hat{\nu}] = L_{\text{thr}}$.
- Add a fixed delay to $\hat{\nu}$: $\nu_d = \hat{\nu} + \nu_{\text{off}}$. ($\nu_{\text{off}}$ can be chosen as the mean of $\nu_{\text{ML}} - \hat{\nu}$.)
- Sample all the bit LLRs at ν_d.

The second algorithm uses a first threshold on $L_{\mathcal{T}0}[\nu]$ followed by a second threshold on the time derivative of $L_{\mathcal{T}0}[\nu]$ to locate the peak. The time derivative, $\frac{dL_{\mathcal{T}0}}{dt}$, (or its discrete-time equivalent) is easily computed from the state space model: note that in equations (4) or (5), $\overrightarrow{m}_{X_{\ell,n}^m}$ is the only time-dependent quantity and its derivative can be obtained from the filter descriptions. A peak detection is feasible because $L_{\mathcal{T}0}[\nu]$ is nearly noise-free above the first threshold.

Threshold Plus Peak Detection "THRNPEAK":

- Open a window (ν_1, ν_2) when $L_{\mathcal{T}0}$ stays above the threshold: $L_{\mathcal{T}0}[\nu] \geq L_{\text{thr}}, \nu_1 \leq \nu \leq \nu_2$.
- Identify a zero crossing of $\frac{dL_{\mathcal{T}0}}{dt}$ in the window at ν_d.
- Sample all the bit LLRs at ν_d.

Table II shows the performance for different values of M and E_b/N_0. Simulations were performed on $10,000$ samples for each set (except 1000 samples for $M = 1024$) The table shows the percentage of false detects, η_{fd}, and the percentage of missed detects, η_{md}, for each case. For η_{fd}, false detects from both events (**E1** and **E2**) are accounted for. The threshold and offset are manually fixed for each set of system parameters. The algorithm "THR" shows a high number of false detects, although η_{md} reduces with either M or E_b/N_0. This method has a higher sensitivity to the choice of the offset ν_{off} because the width of the spike gets narrower as M increases. Secondly, the threshold crossing times have a jitter. These two factors make the detection time, ν_d, fall outside the allowed range more often, leading to a higher η_{fd}. These errors are noticeable at higher values of E_b/N_0 in Table II. Although improvements may be obtained by an accurate estimation of ν_{off}, the algorithm "THRNPEAK" offers a better alternative. The algorithm "THRNPEAK" is less sensitive to the choice of the first threshold and performs closer to "ML" as M or E_b/N_0 are increased. For each choice of E_b/N_0 there exists a value of M above which the detection performance shows considerable improvement. Alternately, at higher values of M, even though the tolerance in (7) is tighter, a given detection performance is achieved at lower value of E_b/N_0. The uncoded BER performance due to timing errors incurs no significant loss in this scheme and stays within the previously mentioned limits. Another observation (not shown in the table) is, the false detects are mostly dominated by the event **E2** discussed before; otherwise ν_d is equal to the true value ν_0 with high probability.

TABLE II
SYNCHRONIZATION AND DETECTION PERFORMANCE

(a) $E_b/N_0 = 2$dB

M	ML η_{fd}	THR η_{fd}	THR η_{md}	THRNPEAK η_{fd}	THRNPEAK η_{md}
128	23.88	99.25	0.35	93.89	0.56
256	9.32	98.32	0.02	83.95	0.05
512	1.62	33.93	0	12.07	0.05
1024	0.1	11.9	0	0.1	0

(b) $E_b/N_0 = 5$dB

M	ML η_{fd}	THR η_{fd}	THR η_{md}	THRNPEAK η_{fd}	THRNPEAK η_{md}
64	16.38	97.78	0.12	89.94	0.19
128	4.41	49.25	0.05	31.87	0.1
256	0.6	19.22	0	1.92	0.01
512	0.01	8.94	0	0	0

(c) $E_b/N_0 = 8$dB

M	ML η_{fd}	THR η_{fd}	THR η_{md}	THRNPEAK η_{fd}	THRNPEAK η_{md}
64	3.38	31.07	0.2	7.2	0.19
128	0.17	15.23	0	0.23	0.03
256	0	25.47	0	0	0
512	0	13.94	0	0	0

(d) $E_b/N_0 = 10$dB

M	ML η_{fd}	THR η_{fd}	THR η_{md}	THRNPEAK η_{fd}	THRNPEAK η_{md}
64	0.58	20.85	0	1.44	0
128	0.02	10.71	0	0.02	0
256	0	37.02	0	0	0
512	0	12.11	0	0	0

VI. CONCLUSION

We have shown that near-optimal synchronization of isolated multicarrier symbols can be obtained as a by-product of matched filtering. The method does not require the sub-carriers to be down-converted before sampling; however, if this is done, then the sensitivity to timing errors would significantly reduce and operation at even lower SNRs may be feasible. Performance improvements are also possible by modulating some sub-carriers with known data. The approach of using glue factor constraints may be extended with some changes to non-binary signaling schemes as well. These are open for further work.

REFERENCES

[1] V. Lottici, M. Luise, C. Saccomando, and F. Spalla, "Non-data-aided timing recovery for filter-bank multicarrier wireless communications," *IEEE Trans. Signal Process.*, vol. 54, no. 11, pp. 4365–4375, Nov 2006.

[2] M. Carta, V. Lottici, R. Reggiannini, and F. Cianchi, "Receiver design for filter-bank multicarrier systems over time-frequency selective channels," in *Vehicular Technology Conference, 2007. VTC2007-Spring. IEEE 65th*, Apr. 22–25, pp. 2359–2363.

[3] H.-A. Loeliger, L. Bolliger, C. Reller, and S. Korl, "Localizing, forgetting, and likelihood filtering in state-space models," in *Information Theory & Applications Workshop*, UCSD, La Jolla, Feb. 8–13 2009.

[4] H.-A. Loeliger, J. Dauwels, J. Hu, S. Korl, L. Ping, and F. R. Kschischang, "The factor graph approach to model-based signal processing," in *Proc. IEEE*, vol. 95, no. 6, 2007, pp. 1295–1322.

[5] J. M. Wozencraft and I. M. Jacobs, *Principles of Communication Engineering*. John Wiley & Sons, 1965.

[6] M. Devarakonda, "Joint matched filtering, decoding, and timing synchronization," Ph.D. dissertation, ETH Zurich, 2011, Hartung-Gorre Verlag Konstanz.